A thermomechanical model of multi-shape memory effect for amorphous polymer with tunable segment compositions

Xiaodong Wang[a], Haibao Lu[a,*], Xiaojuan Shi[a], Kai Yu[b] and YongQing Fu[c]

[a]Science and Technology on Advanced Composites in Special Environments Laboratory, Harbin Institute of Technology, Harbin 150080, China

[b]Department of Mechanical Engineering, University of Colorado Denver, Denver, CO 80217, United States

[c]Faculty of Engineering and Environment, University of Northumbria, Newcastle upon Tyne, NE1 8ST, UK

[*]Corresponding author, E-mail: luhb@hit.edu.cn

Abstract: Multi-shape memory effect (multi-SME) in amorphous polymers has attracted great attention due to their complex thermal transitions and multi-step recovery behavior. Many experimental studies have been reported for synthesis, characterization, testing and demonstration of the multi-SME. However, theoretical approaches have seldom been applied although they are critically needed to understand the principles and predict the behavior of the multi-SME in various amorphous polymers. In this study, a new thermomechanical model was proposed to describe the thermo-/chemo-responsive multi-SME of amorphous polymers with tunable segment compositions. Based on the Weibull statistical model, a new constitutive framework was established to describe temperature-, stretch ratio- and strain-dependent behaviors of thermo-/chemo-responsive multi-SME. Finally, this newly proposed model was applied to quantitatively identify the crucial factors for the

thermo-/chemo-responsive shape recovery behaviors, which have been verified by the reported experimental data.

Keywords: thermomechanical model; composite; multi-shape memory effect

1. Introduction

Shape memory polymers (SMPs) are stimulus-responsive soft materials which could recover their original shapes from the predetermined temporary shapes by means of a suitable environmental stimulus, such as heat, light, electricity, magnetic field or water etc. [1-3]. In comparison with other types of soft materials such as electroactive elastomers and hydrogels, SMPs have unique and desirable shape memory capabilities owing to the pre-stored mechanical energy during the pre-deformation stage [4,5]. In terms of thermodynamics, SMP macromolecules are normally composed of two or more segments, at least one of which is the hard segment and the others of which is soft one [6,7]. A cooperative relaxation could happen between the hard and soft segments at temperatures below and above the glass transition temperature [6-8]. Therefore, shape memory behavior of amorphous SMPs has been theoretically explained based on the thermo-visco-elasticity effects, and the mobility changes in the macromolecules has been linked to the changes in the viscosity or relaxation time using rheological elements [9,10].

For the SMPs with tunable segment compositions, working mechanism of the multi-SME is similar to those of the standard one-stage one with two-segments [11-17]. SME in the SMPs has enabled a variety of applications including deployable structures, biomedical devices, adaptive optical devices, smart sensors and actuators.

Successful applications of the SMPs are strongly dependent upon the number of temporary shapes and the tunable shape memory transition temperature(s) for the targeted applications [1,3,15]. However, it is not straightforward to model the multi-SME due to its complex and dynamic transition of the segment composition [18-25]. Theoretical studies have previously been proposed to model and predict the multi-SME based on different molecule structures and cooperative relaxation [6,7]. In these pioneer studies, the constitutive relations were typically based on a specific modeling frame. For example, in order to explain the sophisticate thermomechanical and recovery behaviors of SMPs, a generalized Maxwell model with multiple non-equilibrium branches was often employed [17,26,27]. Although simulation results using these models were well agreeable with the experimental results, a huge calculation work was often needed due to the considerations of many parameters in the simulation processes. Therefore, this paper aims to establish a phenomenological model from the thermodynamic point of view to explain the working mechanism in the multi-SME of the thermo-/chemo-responsive SMPs with tunable segment compositions. Based on a Weibull statistical model, a constitutive framework was established to describe the temperature-, stretch ratio- and strain-dependent behaviors of thermo-/chemo-responsive SMEs. Finally, the thermomechanical model was applied to quantitatively identify the key factors of multi-SME, and then verified using the experimental data reported in the literature.

2. Viscoelastic behavior and theoretical modeling of SME

SMPs exhibit unique thermodynamics properties and respond to the environmental

and temperature changes. They were often characterized using dynamic mechanical analysis (DMA) tests, and thus the viscoelastic behavior was often expressed as a function of storage modulus [28-30]. Therefore, storage modulus is a key function to reflect the thermomechanical properties of SMPs. Weibull statistical model was previously used to explain thermomechanical transitions of the amorphous polymers and their relaxation behaviors of the macromolecules as a function of temperature [31]. This model has the following form,

$$E(T)=(E_1\text{-}E_2)\cdot\exp\left(-(\frac{T}{T_\beta})^{m_1}\right)+(E_2\text{-}E_3)\cdot\exp\left(-(\frac{T}{T_g})^{m_2}\right)+E_3\cdot\exp\left(-(\frac{T}{T_f})^{m_3}\right) \quad (1)$$

where E_i (i=1, 2, 3) is the moduli of the amorphous polymers at a temperature below, at and above glass transition temperature (T_g); m_i represents the Weibull statistics of the bond breakage; T_β and T_f are the temperatures below and above T_g, respectively.

For the SMPs, the transition temperature range of $T_g \pm 15^oC$ is considered to cover the applicable range for the shape recovery. The transition temperature is much higher than the T_β, but lower than the T_f, so the term of $\exp\left(-(\frac{T}{T_\beta})^{m_1}\right)$ is close to zero and the term of $\exp\left(-(\frac{T}{T_f})^{m_3}\right)$ is close to 1. Accordingly, equation (1) could be rewritten as follows,

$$E(T)=(\mathrm{E}_2\text{-}\mathrm{E}_3)\cdot\exp\left(-\left(\frac{T}{T_g}\right)^{m_2}\right)+E_3 \quad (2)$$

[Figure 1]

Figure 1 plots the numerical results for the effect of temperature on the modulus

changes of SMPs with different T_g values of 341.8K, 345K, 350K, 355K and 360K, respectively. Experimental data reported in Ref. [40] are also plotted for comparisons. The fitting parameters are E_2=1053.41MPa, E_3=44.11MPa and m_2=41, which show that the simulation results are in good agreements with the experimental ones. The modulus is gradually decreased with an increase in temperature. With the T_g increased from 341.8K, 345K, 350K, 355K to 360K, the modulus of the SMP is increased at the same testing temperature. Therefore, a higher modulus of the SMP is linked with a higher T_g of the SMP according to the equation (2). The simulation results confirm that the thermomechanical property is strongly determined by the T_g. If the transition temperature is decreased, the modulus of the SMP is therefore decreased.

Equation (2) shows that the SME is determined by both the thermomechanical and viscoelastic properties of the polymer macromolecules and their segments. Therefore, the shape memory behavior of amorphous SMPs has been studied via the relaxation time using the rheological elements, which have been previously reported [9,10]. The Arrhenius rule, Williams-Landel-Ferry (WLF) equation and Vogel-Fulcher-Tammann rule [27,32-34] have therefore been employed to model and predict the relaxation behavior of SMPs. The constitutive relationship between the relaxation time (τ) and the external stress σ at a given temperature can be written as [35],

$$\tau = \tau^{ref} \exp(\frac{-\Delta G + \alpha\sigma}{RT}) \tag{3}$$

where ΔG is the Gibbs energy of activation, τ^{ref} is the reference relaxation time and α is a constant associated with the polymer material.

Meanwhile, the modulus of the polymer could also be determined by the relaxation time [34], which can be written as,

$$E_2 = E_2^{ref} \exp(\frac{-\Delta G+\alpha\sigma}{RT}) \tag{4}$$

where E_2 is the modulus of the polymer at the glass transition stage and is the initial modulus at the beginning of the glass transition.

According to the previous work [36], not only the modulus of the polymer, but also T_g is significantly influenced by the stress. Boyer proposed a linear model based on the experimental data to express this phenomenon, which has the form as [37],

$$T_g = A - B\sigma \tag{5}$$

where A and B are the given constants. When the temperature range is limited to T_g $\pm$15K, the E_3 has insignificant influence on the gloss modulus. Therefore, E_3 is assumed to be a constant during the glass transition progress. Here, the relationship between the modulus and stress is obtained by substituting equations (4) and (5) into equation (2), which results in,

$$E(T,\sigma) = \left(E_2^{ref} \exp(\frac{-\Delta G+\alpha\sigma}{RT}) - E_3 \right) \cdot \exp\left(-(\frac{T}{A-B\sigma})^{m_2} \right) + E_3 \tag{6}$$

According to the relationship of $\sigma = E(T,\sigma)\cdot\varepsilon$, the resulting strain ε is given by,

$$\varepsilon = \sigma / \left(\left(E_2^{ref} \exp(\frac{-\Delta G+\alpha\sigma}{RT}) - E_3 \right) \cdot \exp\left(-(\frac{T}{A-B\sigma})^{m_2} \right) + E_3 \right) \tag{7}$$

Based on the previously published work about the effect of stress on the strain for amorphous polymers [38], the experimental results are employed to verify our theoretical model. Table 1 presents the parameter values of the polymer with T_g

=340K. The theoretical results obtained based on equation (7) and experimental data of the storage modulus are plotted in Figure 2 for comparisons. It is found that the simulation results are in good agreements with those of the experimental ones for the SMP under stress values of 1.5 MPa and 3.0 MPa. For a given stress, a larger strain (e.g., deformation) is linked with an increase in the temperature. Furthermore, the changes in strain become significant as the SMP is heated to the $T_g \pm 15$K. These simulation results could also be explained by the effect of temperature on the thermomechanical property (e.g., modulus). The modulus will be decreased with increasing the temperature of the SMP, thus resulting in a larger strain under a given constant stress, based on the origin of the constitutive relation of $\varepsilon=\sigma/E$. These simulation results confirm that the constitutive relationships among the strain, temperature and stress can be explained using the equation (7) to characterize the thermomechanical behavior of the SMP.

[Table 1]

[Figure 2]

For the SMPs, the stretch ratio is an important time-dependent parameter to describe their relaxation behaviors. The relaxation time always plays an essential role to determine the viscoelastic behavior and thermomechanical properties of the SMPs. According to the WLF equation [27], effect of time on the relaxation behavior of the SMP has a similar effect as that of temperature. Therefore, the stretch ratio dependence of the T_g can be described by,

$$T_g = T_g^{ref} + \frac{c_2 \log(\varepsilon / \varepsilon^{ref})}{c_1 - \log(\varepsilon / \varepsilon^{ref})} \tag{8}$$

where T_g^{ref} is the referenced glass transition temperature, c_1 and c_2 are the given constants, ε is the stretch ratio and ε^{ref} is the referenced stretch ratio at the T_g^{ref}.

The characteristic modulus as a function of stretch ratio can be expressed using,

$$E_i = E_i^{ref}\left(1 + s_i \log\left(\frac{\varepsilon}{\varepsilon^{ref}}\right)\right) \tag{9}$$

where s_i is the given constant.

By combining equations (2), (8) and (9), we obtain,

$$E(T,\varepsilon) = \left(E_2^{ref}\left(1 + s_2 \log\left(\frac{\varepsilon}{\varepsilon^{ref}}\right)\right) - E_3\right) \cdot \exp\left(-\left(T / (T_g^{ref} + \frac{c_2 \log(\varepsilon / \varepsilon^{ref})}{c_1 - \log(\varepsilon / \varepsilon^{ref})})\right)^{m_2}\right) + E_3 \tag{10}$$

To characterize the effect of frequency on the modulus, equation (10) can be further written as,

$$E(T,\varepsilon) = \left(E_2^{ref}\left(1 + s_2 \log\left(\frac{f}{f^{ref}}\right)\right) - E_3\right) \cdot \exp\left(-\left(T / (T_g^{ref} + \frac{c_2 \log(f / f^{ref})}{c_1 - \log(f / f^{ref})})\right)^{m_2}\right) + E_3 \tag{11}$$

Based on equation (11), the relationship between storage modulus and temperature is compared with the experimental results obtained from the styrene-based SMP[38], which have been presented in Figure 3. The values of the parameters in equation (11) are presented in Table 2. It is found that the storage modulus is gradually increased with an increase in the frequency at the same temperature. That is to say, the storage modulus will be increased by decreasing the stretch ratio. A good agreement between

the simulation and experimental results supports that the equations (10) and (11) are able to predict the thermomechanical behavior of the SMPs. This model could not only predict the change in thermomechanical performance, but also qualitatively separate the effect of frequency (or stretch ratio) on the T_g determined by the constitutive relationship between $E(T,\varepsilon)$ and temperature.

[Table 2]

[Figure 3]

3. Working mechanism and theoretical modeling of multi-SME

The multi-SME refers to the phenomenon that a SMP has the capability to memorize multiple temporary shapes in a single shape memory cycle [15-17]. With more than one soft segment and one hard segment, a SMP could have the multi-SME. Here, we assume that the role of soft segments is similar to that in a dual-segment polymer system, thus the working mechanism of the multi-SME is similar to that for the dual-segment polymer system. We can then formulate the constitutive relationship for the modulus and temperature to characterize the thermomechanical properties of the SMPs with the multi-SME. Based on the Takayanagi principle [6,21,22], different soft segments are in parallel connections and the normalized length is equal to each other. While the proportion of different soft segments can be represented by the normalized cross-sectional area (ϕ_i). Equation (11) can be rewritten in a parallel form by Boltzmann superposition principle [26,27],

$$E(T,f)=\left\{\sum_{i=1}^{n}\phi_i \Big/ \left(\begin{array}{l}\left(E_2^{ref}(i)\left(1+s_2(i)\log\left(\dfrac{f}{f^{ref}(i)}\right)\right)-E_3(i)\right)\cdot \\ \exp\left(-\left(T/(T_g^{ref}(i)+\dfrac{c_2^{ref}\log(f/f^{ref}(i))}{c_1^{ref}-\log(f/f^{ref}(i))})\right)^{m_2(i)}\right)+E_3(i)\end{array}\right)\right\}^{-1} \quad (12)$$

where n is the number of the soft segments.

Meanwhile, if the soft segments are in series connections, the normalized cross-sectional area is then assumed as being equal to each other. The proportion of different soft segments can then be represented by the normalized length (λ_i) of the segment. Here equation (11) has a series form as follows,

$$E(T,f)=\sum_{i=1}^{n}\lambda_i\left(\begin{array}{l}\left(E_2^{ref}(i)\left(1+s_2(i)\log\left(\dfrac{f}{f^{ref}(i)}\right)\right)-E_3(i)\right)\cdot \\ \exp\left(-\left(T/(T_g^{ref}(i)+\dfrac{c_2^{ref}\log(f/f^{ref}(i))}{c_1^{ref}-\log(f/f^{ref}(i))})\right)^{m_2(i)}\right)+E_3(i)\end{array}\right) \quad (13)$$

We firstly studied a SMP with triple-segments, and then extended the model to the SMP with more general multi-segment compositions. For the SMP with triple-segments, it is assumed that the SMP has two values of T_g, where $T_g^{ref}(1)$ =340K and $T_g^{ref}(2)$=400K. The effect of the temperature on the modulus ($\log E$) is revealed in Figures 4(a) and 4(b), at two different frequencies of f =0.01Hz and f =100Hz, respectively. For the two situations of series and parallel connections, the relationships between the modulus (E/E_{S1}) of polymer with the temperature is plotted. For a given frequency applied on the SMP with triple-segments, the modulus of the polymer gradually decreases with the increase in temperature. The simulation curves for both series and parallel connections reveal two stages of thermal transitions around $T_g^{ref}(1)$=340K and $T_g^{ref}(2)$=400K. The T_g of the first soft segment is found

to be increased from 348K to 370K with an increase in the frequency from 0.01Hz to 100Hz. The same trend could be found for the thermal transition of the second soft segment for the SMPs with triple-segment composition.

[Figure 4]

The above results show that the parallel connection model is better to show the plateau state to indicate a clear multi-SME in SMPs. Therefore, equation (12) is further employed to investigate the effect of the cooperatively thermal transitions of the soft segments on the thermomechanical property. Figure 5 shows five relaxation curves in which the modulus ($\log E$) is plotted *versus* temperature at different T_g values of $T_g^{ref}(1)$ and $T_g^{ref}(2)$. Figures 5(a) and 5(b) shows the effects of $T_g^{ref}(1)$ (330K, 340K, 350K, 360K or 370K) and $T_g^{ref}(2)$ (350K, 360K, 370K, 380K or 390K) for the soft segments on the modulus, respectively. Figures 5(a) shows that the plateau range becomes narrower with an increase in the $T_g^{ref}(1)$, thus resulting in a smaller temperature difference between the $T_g^{ref}(1)$ and $T_g^{ref}(2)$. The similar changes can also be found in Figures 5(b), e.g., the plateau range becomes wider with an increase in the $T_g^{ref}(2)$, thus resulting in a larger temperature difference between the $T_g^{ref}(1)$ and $T_g^{ref}(2)$. These simulation results clearly show that a wider plateau is generated if there is wider transition temperature difference between the two soft segments. This has been well-documented in the experimental work on the structural designs of the multi-SME in SMPs. If the DMA testing is used for determining the multi-SME, we need to choose the SMPs with triple-segments or multi-SME, and a larger temperature difference interval between the $T_g^{ref}(1)$ and $T_g^{ref}(2)$. Finally, it

should be noted that the thermomechanical property of the soft segment is only determined by its T_g, but not by the transition temperature of the other soft segments. The thermomechanical property of the SMPs is determined by the cooperative interaction of the soft segments.

[Figure 5]

Boltzmann superposition principle [26,27] is now employed to characterize the cooperative relaxation effect on the thermomechanical property of the SMPs with multi-segment compositions. Equation (2) can be rewritten as,

$$E(T)=\left(\sum_{i=1}^{n}\phi_i / \left(\left(E_2(i)-E_3(i)\right)\cdot\exp\left(-\left(T/T_g(i)\right)^{m_2(i)}\right)+E_3(i)\right)\right)^{-1} \quad (14)$$

Figure 6 plots the numerical results obtained from equation (14) for the effect of temperature on the modulus of SMP, together with the experimental data reported in ref. [39] for a comparison. All the given constant values of the parameter used in equation (14) are listed in Table 3. It is found that the simulation results could well predict the experimental ones. A comparison between results from both the proposed model and experimental work supports that the proposed model could well simulate and predict the multi-SME of the SMPs. Figure 6 shows the results for the SMP with triple segments (one hard segment and two soft ones). It indicates that the two segments trigger two-stage shape recovery and glass transition in the SMP according to the theoretical curve, although the experimental results did not present a clear changes of two-stage shape recovery and glass transition. This indicates that the theoretical model could be used to identify and predict the multi-SME and multi-glass transition in SMPs. It is expected that this phenomenon happens apparently in the

second-stage phase transition process similar with the first one for the SMPs with two soft segments.

[Table 3]

[Figure 6]

4. Modelling of thermo-/chemo-responsive multi-SME

Essentially, the mechanism of chemo-responsive SME in the SMPs is similar to that of the thermo-responsive one [40]. However, instead of being heated above the transition temperature of the SMPs, the chemo-responsive SME is resulted from the decrease of transition temperatures induced by plasticizing or swelling effect [41,42]. Here we modified our proposed model in order to predict the chemo-responsive multi-SME. As is well known, absorption of solvent molecules has a similar effect with the reduction of the transition temperature of polymer due to the plasticizing effect [41]. The effect of the absorption of small molecules on the transition temperature can be expressed using the following equation [41],

$$\Delta T = \beta n_1 \tag{15}$$

where n_1 is the mole number of solvent molecules and β is defined as a proportional factor.

In order to calculate the numbers of the absorption of the solvent molecules, $V(t)$ is introduced and is the volume of the polymer/solvent mixture at the time of t, while labels 1 and 2 represent that the corresponding parameters are for solvent and polymer, respectively.

It is assumed that both polymer and solvent molecules are incompressible. When

the solvent molecules are diffused into polymer, the volume of the cubic polymer is changed from 1 to a value of $V(t)$. The symbols about stretching, e.g., λ_1, λ_2 and λ_3 are used to represent the dimension changes of the cubic polymer in three directions. As the polymer is stretched without a constraint, e.g., $\lambda_1 = \lambda_2 = \lambda_3 = \lambda$, the volume parameter can be expressed as,

$$V(t)=\lambda^3 \tag{16}$$

According to the lattice theory [42], the volume of a polymer molecule is *m* times as high as that of the solvent molecule. Therefore, the volume fraction of solvent can be further written as,

$$\phi_1(t)=\frac{n_1}{n_1+mn_2}=\frac{V(t)-1}{V(t)}=\frac{\lambda^3\text{-}1}{\lambda^3} \tag{17}$$

where n_1 and n_2 are the molar numbers of the solvent and polymer, respectively, and $\phi_1(t)$ is the volume fraction of solvent.

As n_2 is a constant during the mixing process, equation (17) can be further written as,

$$n_1 = mn_2\lambda^3 - mn_2 \tag{18}$$

The relationship between the transition temperature and molar number of solvent can be obtained by incorporating equation (18) into (15), therefore, we now have,

$$\Delta T = \beta mn_2\lambda^3 - \beta mn_2 \tag{19}$$

The function $\gamma = \beta mn_2$ is introduced to simplify equation (19),

$$\Delta T = \gamma\lambda^3 - \gamma \tag{20}$$

The stretch ratio is equal to the stretch ratio, which can be written as,

$$\frac{\bar{\varepsilon}}{\varepsilon^{ref}} = \frac{\bar{\lambda}}{\lambda^{ref}} \tag{21}$$

where λ^{ref} is the referenced stretch ratio.

Combining equations (7), (20) and (21), we have obtained,

$$T_g = T_g^{ref} + \frac{c_2^{ref}\log(\bar{\lambda}/\lambda^{ref})}{c_1^{ref} - \log(\bar{\lambda}/\lambda^{ref})} - \gamma\lambda^3 + \gamma \tag{22}$$

Figure 7(a) plots the numerical results for the relationship of transition temperature ($T_g - T_g^{ref}$) and stretch (λ) of the polymer mixed with the solvent. At different stretch ratios of $\bar{\lambda}$=0.001, 0.01, 0.1, 1 or 10, transition temperatures of the polymer are gradually decreased by increasing the stretch ratio under a given stretch value. The numerical results reveal that the stretch ratio has a significant effect on the changes of transition temperatures for the SMP. Furthermore, as the transition temperature is decreased to a certain value, the stored mechanical energy in the polymer is released, and accordingly the SME is triggered [43-47]. As an example, the T_g is increased with a value of 10K when the frequency is increased from 0.001Hz to 10Hz. Results show that the T_g is gradually increased if the frequency is applied on the polymer. Furthermore, Figure 7(b) shows the relationship between transition temperature ($T_g - T_g^{ref}$) and $\gamma(K)$ for SMP in order to study the effect of molar number on the T_g. It is found that the transition temperature ($T_g - T_g^{ref}$) is gradually decreased with the function ($\gamma(K)$) is increased from 0 to 10, which is mainly attributed to the plasticizing effect of solvent on the SMP, according to equation (15).

[Figure 7]

In this section, we will further qualitatively investigate the swelling-induced shape

recovery. Firstly, rubber elastic theory is employed to theoretically identify the effect of volume changes on the activation enthalpy values of the SMP. When a polymer absorbs the solvent molecules, it is swollen until an equilibrium is reached during the swelling [43]. However, it is difficult to use our model to predict the swollen driven instability and buckling of the chemo-responsive SME, which have been previously reported in the literature [44,45]. This is simply because our model is employed to characterize the thermomechanical properties of the SMPs. The polymer concentration in the mixture (from n_2 to $\frac{1}{\lambda^3}n_2$, while the initial volume of the polymer is assumed to be normalized dimensionless function of $V(0)=1$ and the swollen volume is to be $V(t)=\lambda^3$) has an apparent effect on the activation enthalpy, which can be expressed as,

$$\Delta H_{dry} = \lambda^3 \Delta H_{wet} \tag{23}$$

where ΔH_{dry} and ΔH_{wet} are the activation enthalpy values of the dry and swollen SMPs, respectively.

Shape memory behavior of the SMP is governed by WLF rule [11,17,26,27], and accordingly the relationship between modulus and activation enthalpy can be expressed as,

$$E_2 = E_2^{ref} \exp(\frac{\Delta H_{dry}}{\lambda^3 RT}) \tag{24}$$

where R is the universal gas constant, E_2^{ref} and E_2 are the moduli of dry and swollen SMPs, respectively.

After substituting equations (21) and (24) into equation (8), we have

$$E_2 = E_2^{ref} \exp\left(\frac{\Delta H_{dry}}{\lambda^3 RT}\right)\left(1+s_i \log\left(\frac{\bar{\lambda}}{\bar{\lambda}^{ref}}\right)\right) \tag{25}$$

Here, by combining equations (22), (25) and (9), we obtain:

$$E_2(T,\bar{\lambda}) = E_2^{ref}\left(1+s_2 \log\left(\frac{\bar{\lambda}}{\bar{\lambda}^{ref}}\right)\right)\cdot \exp\left(\left(\frac{\Delta H_{dry}}{\lambda^3 RT}\right)-\left(\frac{T}{T_g^{ref}+\frac{c_2^{ref}\log(\bar{\lambda}/\bar{\lambda}^{ref})}{c_1^{ref}-\log(\bar{\lambda}/\bar{\lambda}^{ref})}-\gamma\lambda^3+\gamma}\right)^{m_2}\right) \tag{26}$$

where c_1^{ref} =17.44 and c_2^{ref} =51.6K are given constants of the WLF equation.

According to the relationship of the strain (λ) and stretch ratio ($\bar{\lambda}$), combining equations (20), (24) and (2), we can obtain,

$$E(T,\lambda) = E_2 \cdot \exp\left(\left(\frac{\Delta H_{dry}}{\lambda^3 RT}\right)-\left(T/(T_g-\gamma\lambda^3+\gamma)\right)^{m_2}\right) \tag{27}$$

In order to quantitatively investigate the effect of swollen volume on the storage modulus, we set the values of γ as γ=0, 10, 20 and 40K. The values of the parameters in equation (27) are listed in Table 4. Based on analytical results of equation (27), the relationship between storage modulus and swollen volume can be obtained and compared with the reported experimental results [43] for comparisons. The results are presented in Figure 8. The simulation results reveal that the storage modulus is gradually decreased with an increase in the swollen volume, which can be well explained using the rubber elastic theory reported in literature [48,49]. With the increases in the swollen volume of polymer and solvent mixture, the concentration of the polymer is therefore decreased, thus resulting in the decrease of both the activation enthalpy and storage modulus.

[Table 4]

[Figure 8]

However, it should be mentioned that the swollen volume is difficult to be measured in practice, whereas the stretch ratio and temperatures can be precisely controlled and their relationship with the storage modulus are easily obtained using experimental methods such as DMA. Therefore, it would be more suitable to investigate the relationships among storage modulus, stretch ratio and temperature, and then compare the theoretical results with experimental ones for further verifications. Figures 9(a) and 9(b) are the obtained theoretical and experimental results. It is found that the storage modulus is gradually increased with an increase in the stretch ratio from λ / λ^{ref} =0.01, 0.1 1, 10, 100 to 1000, as revealed in Figures 9(a). On the other hand, effect of the temperature on the storage modulus is shown in Figures 9(b), which reveals that the storage modulus is gradually decreased with an increase in the temperature. For a given SMP, the storage modulus decreases when the SMP is heated to a higher temperature (from 263K, 273K, 283K, 293K to 303K). The relaxation time is therefore shortened based on the Arrhenius rule, resulting in the earlier initiation of SME and shape recovery.

[Figure 9]

5. Conclusions

In this study, a thermomechanical model was proposed to investigate the unique characteristics and working mechanisms of amorphous SMP with multi-SME and tunable segment compositions. Weibull statistical model was firstly employed to formulate a constitutive framework for the temperature-, stretch ratio- and

strain-dependences of thermo-responsive multi-SME. A thermomechanical model was then proposed to quantitatively identify the key factors behind the thermo-responsive shape recovery behavior, which were verified by the experimental data. The proposed model was further extended to characterize and predict the chemo-responsive SMEs by means of plasticizing and swelling effects, respectively. Good agreements between the simulation and experimental results were obtained. This newly proposed model is expected to provide a powerful tool to understand the working mechanisms for the SMPs with thermo-/chemo-responsive multi-SME and tunable segment compositions.

Acknowledgements

This work was financially supported by the National Natural Science Foundation of China (NSFC) under Grant No. 11672342 and 11725208, Newton Mobility Grant (IE161019) through Royal Society and NFSC.

References

[1] Mather PT, Luo XF, Rousseau IA. Shape memory polymer research. Annu Rev Mater Res 2009;39:445-471.

[2] Lu HB, Yao YT, Huang WM, Hui D. Noncovalently functionalized carbon fiber by grafted self-assembled graphene oxide and the synergistic effect on polymeric shape memory nanocomposites. Compos Part B-Eng 2014;67: 290-295.

[3] Xie T. Recent advances in polymer shape memory polymer. Polymer 2011;52(22):4985-5000.

[4] Lendlein A, Jiang H, Jünger O, Langer R. Light-induced shape-memory polymers. Nature (London) 2005;434(7035):879-882.

[5] Grzemba B. New Experimental investigations on the dieterich-ruina friction law. Facta Universitatis-Series Mechanical Engineering 2015;13:11-20.

[6] Lu HB, Yu K, Huang WM, Leng JS. On the Takayanagi principle for the shape memory effect and thermomechanical behaviors in polymers with multi-phases. Smart Mater Struct 2016;25(12):125001.

[7] Lu HB, Wang XD, Yu K, Huang WM, Yao YT, Leng JS. A phenomenological formulation for shape/temperature memory effect in amorphous polymers with multi stress components. Smart Mater Struct 2017;26(9):095011.

[8] Lu HB, Wang XD, Shi XJ, Yu K, Fu YQ. A phenomenological model for dynamic response of double-network hydrogel composite undergoing transient transition. Compos Part B-Eng 2018;151:148-153.

[9] Voll L. Experimental investigation of the adhesive contact with elastmoers: effect of surface roughness. Universitatis-Series Mechanical Engineering 2015;13:33-8.

[10] Westbrook KK, Kao PH, Castro F, Ding Y, Qi HJ. A 3D finite deformation constitutive model for amorphous shape memory polymers: A multi-branch modeling approach for nonequilibrium relaxation processes. Mech Mater 2011;43(12) :853-869.

[11] Nguyen TD, Qi HJ, Castro F, Long KN. A thermoviscoelastic model for amorphous shape memory polymers: Incorporating structural and stress relaxation. J Mech Phys Solids 2008; 56:2792-2814.

[12] Li GQ, Xu W. Thermomechanical behavior of thermoset shape memory polymer programmed by cold-compression: Testing and constitutive modeling. J Mech Phys Solid 2011;59:1231-1250.

[13] Lu HB, Huang WM, Leng JS. On the origin of Gaussian network theory in the thermo/chemo-responsive shape memory effect of amorphous polymers undergoing photo-elastic transition. Smart Mater Struct 2016;25:065004.

[14] Milahin N, Li Q, Starcevic J. Influence of the normal force on the sliding friction under ultrasonic oscillations. Universitatis-Series Mechanical Engineering 2015;13:27-32.

[15] Xie T. Tunable polymer multi-shape memory effect. Nature (London) 2010;464:267-270.

[16] Sun L, Huang WM. Mechanisms of the multi-shape memory effect and temperature memory effect in shape memory polymers. Soft Matter 2010;6:4403-4406

[17] Yu K, Xie T, Leng JS, Ding YF, Qi HJ. Mechanisms of multi-shape memory effects and associated energy release in shape memory polymers. Soft Matter 2012;8:5687-5695.

[18] Bellin I, Kelch S, Lendlein A. Dual-shape properties of triple-shape polymer networks with crystallizable network segments and grafted side chains. J Mater Chem 2007;17:2885-2891.

[19] Lendlein A, Schmidt AM, Langer R. AB-polymer networks based on oligo(ε-caprolactone) segments showing shape-memory properties. P Natl Acad Sci USA 2001;98:842-847.

[20] Lee BS, Chul CB, Chung YC, Sul KIl, Cho JW. Structure and thermomechanical properties of polyurethane block copolymers with shape memory effect. Macromolecules 2001;34:6431-6437.

[21] Takayanagi M, Imada I, Kajiyama T. Mechanical properties and fine structure of drawn polymers. J Polym Sci 1966;15:263-281.

[22] Takayanagi M, Nitta K. Application of a tie molecule model to the postyielding deformation of crystalline polymers. Macromol Theor Simul 1997;6:181-95.

[23] Quitmann D, Gushterov N, Sadowski G, Katzenberg F, Tiller JC. Solvent-sensitive reversible stress-response of shape memory natural rubber. ACS Appl Mater Inter 2013;5:3504-3507.

[24] Heuwers B, Quitmann D, Hoeher R, Reinders FM, Tiemeyer S, Sternemann C, Tolan M, Katzenberg F, Tiller JC Stress-induced stabilization of crystals in shape memory natural rubber. Macromol Rapid Commun 2013;34:180-184.

[25] Zhao Q, Behl M, Lendlein A. Shape-memory polymers with multiple transitions: complex actively moving polymers. Soft Matter 2013;9:1744-1755.

[26] Yu K, McClung AJW, Tandon GP, Baur JW, Qi HJ. A thermomechanical constitutive model for an epoxy based shape memory polymer and its parameter identifications. Mech Time-Depend Mat 2014;18(2):453-474.

[27] Yu K, Ge Q, Qi HJ. Reduced time as a unified parameter determining fixity and free recovery of shape memory polymers. Nat Commun 2014;5(3066):1-9.

[28] Yao YT, Luo Y, Xu YC, Wang B, Li JY, Deng H, Lu HB. Fabrication and characterization of auxetic shape memory composite foams. Compos B Eng 2018;152:1-7.

[29] Lu HB, Liu YZ, Huang WM, Wang CC, Hui D, Fu YQ. Controlled evolution of surface patterns for ZnO coated on stretched PMMA upon thermal and solvent treatments. Compos B Eng 2018;132:1-9.

[30] Lu HB, Liu YZ, Xu BB, Hui D, Fu YQ. Spontaneous biaxial pattern generation and autonomous wetting switching on the surface of gold/shape memory polystyrene bilayer. Compos B Eng 2017;122:9-15.

[31] Richeton J, Schlatter G, Vecchio KS, Rémond Y, Ahzi S. A unified model for stiffness modulus of amorphous polymers across transition temperatures and strain rates. Polymer 2005;46(19):8194-8201.

[32] Ge Q, Yu K, Ding Y, Qi HJ. Prediction of temperature-dependent free recovery behaviours of amorphous shape memory polymers. Soft Matter 2012;8(43):11098-11105.

[33] Diani J, Gilormini P, Frédy C, Rousseau I. Predicting thermal shape memory of crosslinked polymer networks from linear viscoelasticity Int J Solids Struct 2012;49(5):793-799.

[34] Lu HB, Huang WM, Leng JS. On the origin of Vogel-Fulcher-Tammann Law in the thermo-responsive shape memory effect of amorphous polymers. Smart Mater Struct 2013;22(10):105021.

[35] Bower DI. An introduction to polymer physics. Cambridge: Cambridge University Press, 2002;188-195.

[36] WARD IM. Mechanical properties of solid polymers. New York: John Wiley&Sons, 1983;86-98.

[37] Boyer RF. The relation of trnasition temperatures to chemical structure in high polymers. Rubber Chem Technol 1963;36(5):1303-1421.

[38] Guo XG, Liu LW, Liu YJ, Zhou B, Leng JS. Constitutive model for a stress- and thermalinduced phase transition in a shape memory polymer. Smart Mater Struct 2014;23(10):105019.

[39] Xie T, Xiao XC, Cheng YT. Revealing triple-shape memory effect by polymer bilayers. Macromol Rapid Commun 2009;30:1823-1827.

[40] Kumpfer JR, Rowan SJ. Thermo-, photo-, and chemo-responsive shape-memory properties from photo-cross-linked metallo-supramolecular polymers. J Am Chem Soc 2011;133(32): 12866-12874.

[41] Lu HB, Liu YJ, Leng JS, Du SY. Qualitative separation of the effect of solubility parameter on the recovery behavior of shape-memory polymer. Smart Mater Struct 2009;18(8):085003.

[42] Lu HB. A simulation method to analyze chemo-mechanical behavior of swelling-induced shape-memory polymer in response to solvent. J Appl Polym Sci. 2012;123(2):1137-1146.

[43] Lu HB, Liu YJ, Leng JS, Du SY. Qualitative separation of the physical swelling effect on the recovery behavior of shape memory polymer. Eur Polym J 2010;46(9):1908-1914.

[44] Huang WM, Lu HB, Zhao Y, Ding Z, Wang CC, Zhang LJ, Sun L, Fu J, Gao XY. Instability/collapse of polymeric materials and their structures in stimulus-induced shape/surface morphology switching. Mater Design 2014;59:174-192.

[45] Salvekar AV, Huang WM, Xiao R, Wong YS, Venkatraman SS, Tay KH, Shen ZX. Water-responsive shape recovery induced buckling in biodegradable photo-cross-linked poly (ethylene glycol)(PEG) hydrogel. Accounts Chem. Res. 2017;50:141-150.

[46] Zhao YJ, Zhao KY, Li Y, Liu L, Zhang XX, Li JG, Chen M, Wang XL. Enrichment of Cd2+ from water with a calcium alginate hydrogel filtration membrane. Sci. China Technol. Sc. 2018;61(3):438-445.

[47] Wang Q, Zhang YY, Dai XY, Shi XH, Liu WG. A high strength pH responsive supramolecular copolymer hydrogel. Sci. China Technol. Sc. 2017;60(1):78-83.

[48] Hudgin DE. Rubber elasticity. New York: Marcel Dekker, Inc. 2000;123-153.

[49] Morton M. Solution theory of polymer. Weinheim: Wiley-VCH. 1987;37-65.

Tables caption

Table 1. The values of the parameters in equation (7)

Table 2. The values of the parameters in equation (11)

Table 3. The values of the parameters in equation (14)

Table 4. The values of the parameters in equation (27)

Table 1. The values of the parameters in equation (7)

E_2^{ref} (MPa)	ΔG (J/mol)	α (J/(mol*MPa)	E_3 (MPa)	A (K)	B (K/MPa)	m_2
1000	14136.6	1341.7	5	340	4.2	55

Table 2. The values of the parameters in equation (11)

E_2^{ref} (MPa)	s_2	f^{ref} (Hz)	$E_3(MPa)$	T_g^{ref} (K)	c_1	c_2	m_2
1014.73	0.025	10	5	333.36	8.39	51.68	36

Table 3. The values of the parameters in equation (14)

ϕ_1	$E_2(1)$ (MPa)	$E_3(1)$ (MPa)	$T_g(1)$ (K)	$m_2(1)$	$E_2(2)$ (MPa)	$E_3(2)$ (MPa)	$T_g(2)$ (K)	$m_2(2)$
0.44	2565.12	30.00	307.07	41	2520.42	20.00	335	53

Table 4. The values of the parameters in equation (27)

ΔH_{dry} (J/mol)	T_g (K)	E_2 (MPa)	γ (K)	m_2
683.76	312.04	7824.63	31.89	20

Figures caption

Figure 1. Moduli of SMP as a function of temperature with T_g of 341.8K, 345K, 350K, 355K and 360K. A comparison is shown between the experimental data obtained from reference [40] and the fitting plots of equation (2) at a T_g of 341.8K of a polystyrene based SMP

Figure 2. A comparison between the simulation and experimental results of the strain as a function of temperature under stress values of 1.5MPa and 3MPa

Figure 3. Storage modulus as a function of the temperature in SMPs with a constant frequency of 0.01Hz, 0,1Hz, 1Hz and 10Hz. (Comparison between experimental result from Ref. [38] and equation (11) in this study)

Figure 4. Modulus $\log E$ as a function of temperature of the SMP with triple-segment, and the simulation results of the series and parallel connection models. (a) At a given constant of f =0.01Hz. (b) At a given constant of f =100Hz

Figure 5. Modulus ($\log E$) as a function of temperature (T) at a given T_g of the soft segments (a) $T_g^{ref}(1)$=330K, 340K, 350K, 360K and 370K. (b) $T_g^{ref}(2)$=350K, 360K, 370K, 380K and 390K

Figure 6. Modulus as a function of temperature for the SMP with a triple-segment. A comparison is shown between the previous experimental data obtained from reference [39] and the fitting plots of equation (14)

Figure 7. Numerical results for the SMP immersed in a solvent. (a) Relation of transition temperature ($T_g - T_g^{ref}$) as a function of strain for a given stretch ratio λ

=0.001, 0.01, 0.1, 1and 10. (b) Relation of transition temperature ($T_g - T_g^{ref}$) as a function of stretch ratio and $\gamma(K)$ function

Figure 8. Storage modulus as a function of swollen volume for the SMP/solvent mixture. A comparison is shown between the experimental data obtained from reference [43] and the fitting plots of equation (27)

Figure 9. Numerical simulation for the relation between the storage modulus as a function of swollen volume of the polymer/solvent mixture. (a) λ/λ^{ref} =0.01, 0.1 1, 10, 100 and 1000; (b) *T*=263K, 273K,283K,293K and 303K

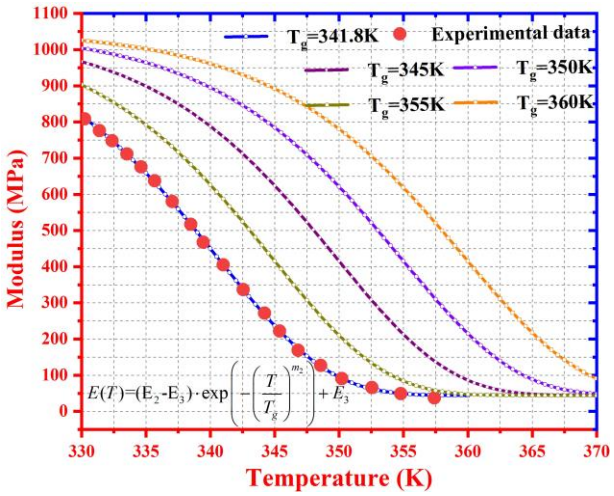

Figure 1. Moduli of SMP as a function of temperature with T_g of 341.8K, 345K, 350K, 355K and 360K. A comparison is shown between the experimental data obtained from reference [40] and the fitting plots of equation (2) at a T_g of 341.8K of a polystyrene based SMP

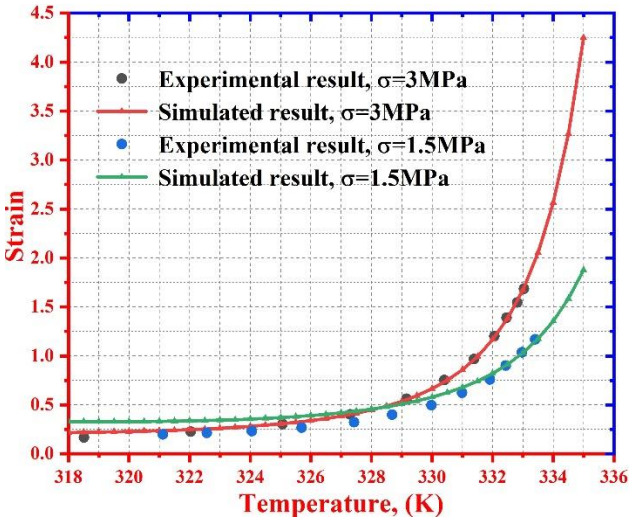

Figure 2. A comparison between the simulation and experimental results of the strain as a function of temperature under stress values of 1.5MPa and 3MPa

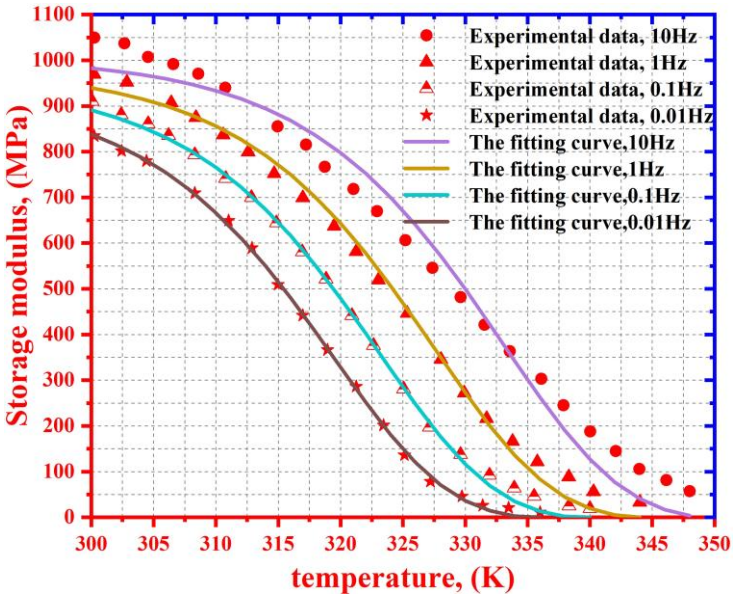

Figure 3. Storage modulus as a function of the temperature in SMPs with a constant frequency of 0.01Hz, 0,1Hz, 1Hz and 10Hz. (Comparison between experimental result from Ref. [38] and equation (11) in this study)

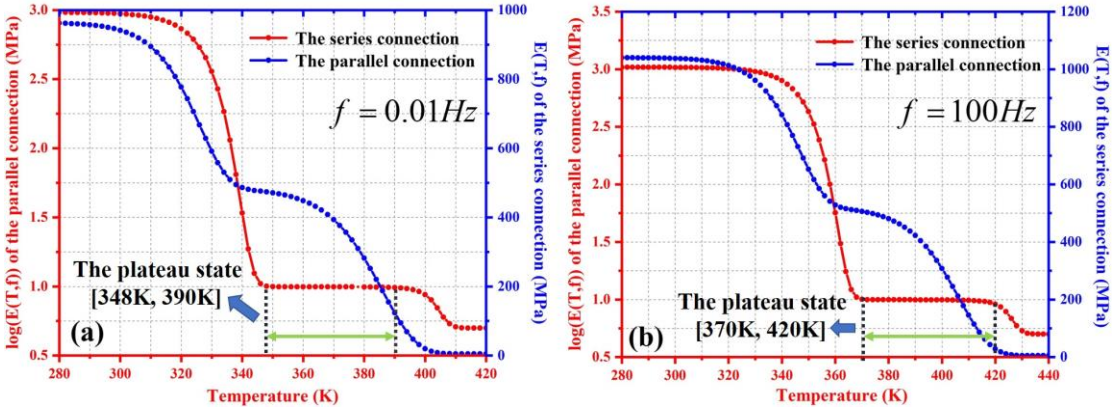

Figure 4. Modulus $\log E$ as a function of temperature of the SMP with triple-segment, and the simulation results of the series and parallel connection models. (a) At a given constant of f =0.01Hz. (b) At a given constant of f =100Hz

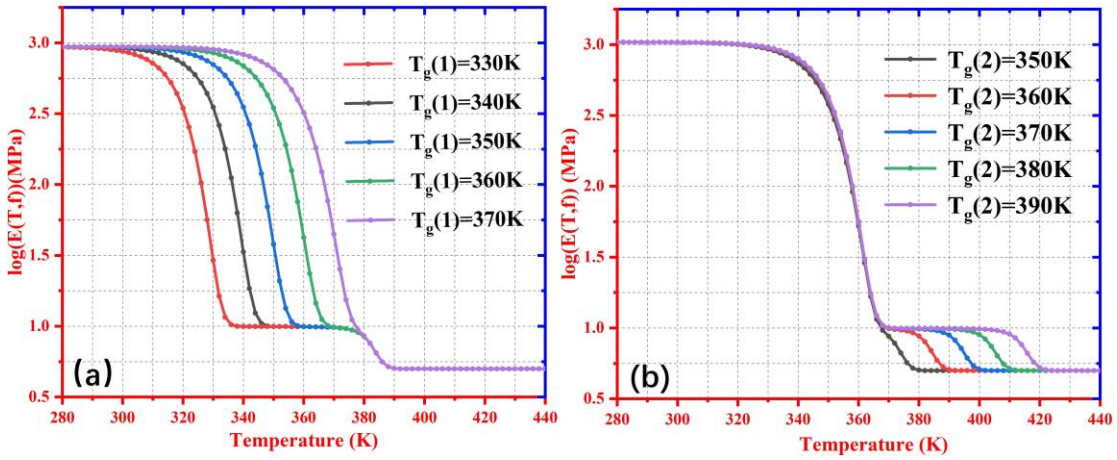

Figure 5. Modulus ($\log E$) as a function of temperature (T) at a given T_g of the soft segments (a) $T_g^{ref}(1)$=330K, 340K, 350K, 360K and 370K. (b) $T_g^{ref}(2)$=350K, 360K, 370K, 380K and 390K

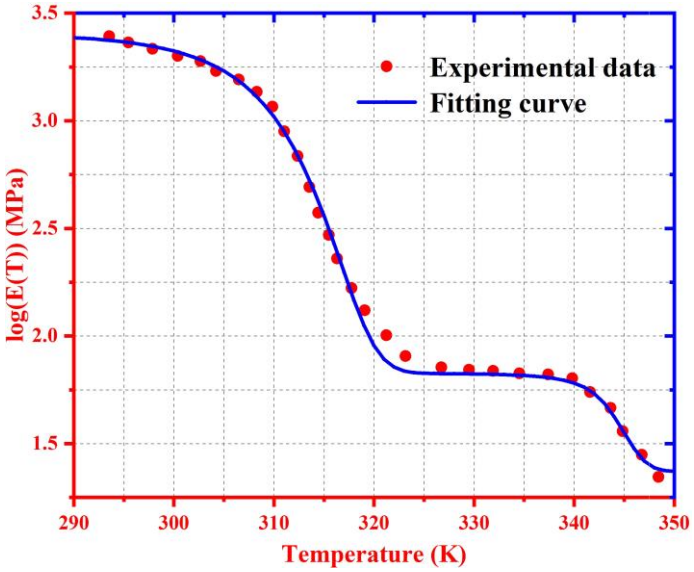

Figure 6. Modulus as a function of temperature for the SMP with a triple-segment. A comparison is shown between the previous experimental data obtained from reference [39] and the fitting plots of equation (14)

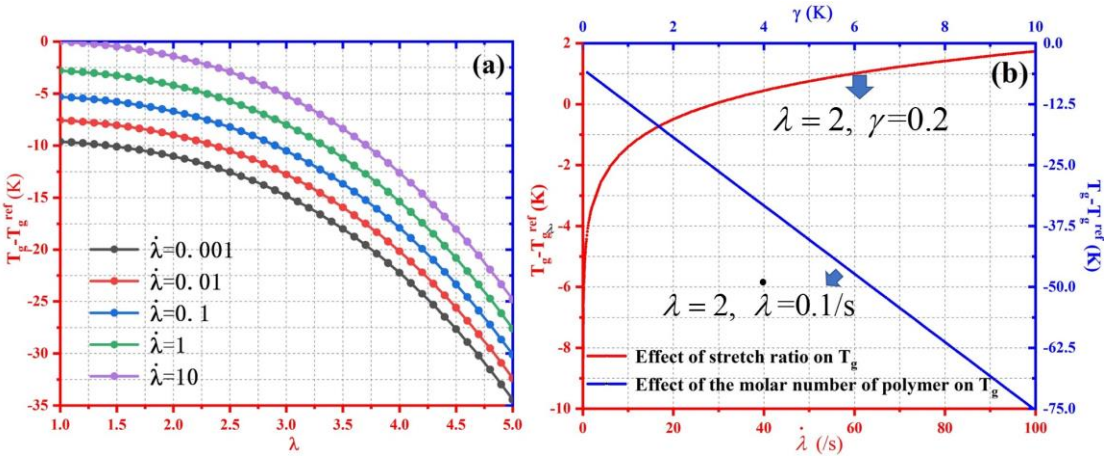

Figure 7. Numerical results for the SMP immersed in a solvent. (a) Relation of transition temperature ($T_g - T_g^{ref}$) as a function of strain for a given stretch ratio $\dot{\lambda}$ =0.001, 0.01, 0.1, 1and 10. (b) Relation of transition temperature ($T_g - T_g^{ref}$) as a function of stretch ratio and $\gamma(K)$ function

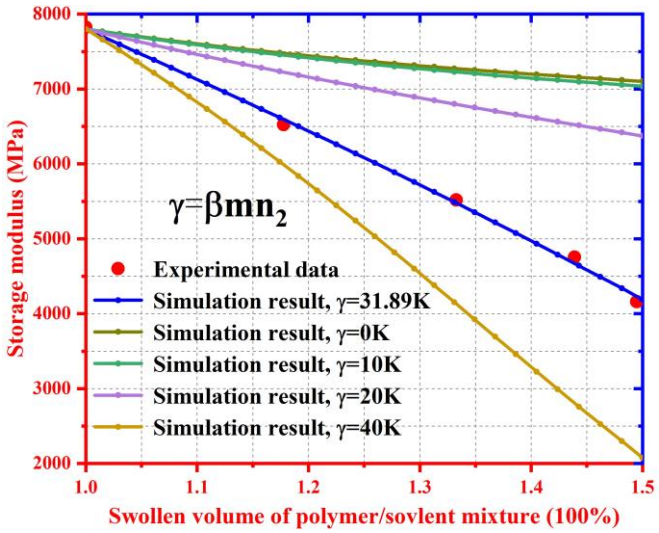

Figure 8. Storage modulus as a function of swollen volume for the SMP/solvent mixture. A comparison is shown between the experimental data obtained from reference [43] and the fitting plots of equation (27)

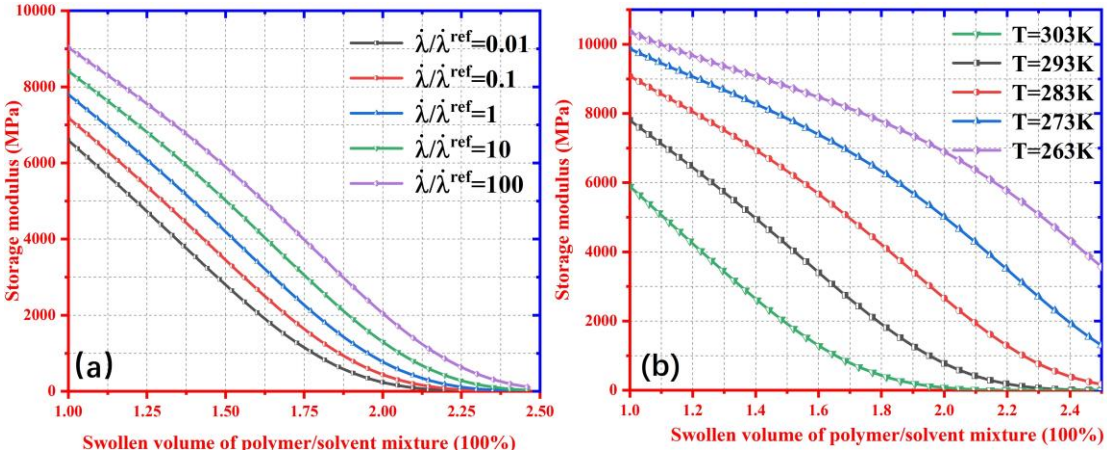

Figure 9. Numerical simulation for the relation between the storage modulus as a function of swollen volume of the polymer/solvent mixture. (a) $\dot{\lambda}/\dot{\lambda}^{ref}$ =0.01, 0.1 1, 10, 100 and 1000; (b) *T*=263K, 273K,283K,293K and 303K